1   To be submitted to Antimicrobial Agents and Chemotherapy

2   **6',6'-Difluoro-aristeromycin is a potent inhibitor of MERS-coronavirus replication**

3

4   Natacha S. Ogando[1], Jessika C. Zevenhoven-Dobbe[1], Dnyandev B. Jarhad[2], Sushil Kumar Tripathi[2], Hyuk

5   Woo Lee[3], Lak Shin Jeong[2], Eric J. Snijder[1#], Clara C. Posthuma[1]*

6

7   [1] Molecular Virology Laboratory, Department of Medical Microbiology, Leiden University Medical Center,

8   Leiden, The Netherlands

9   [2] Research Institute of Pharmaceutical Sciences, College of Pharmacy, Seoul National University, Seoul

10   08826, Korea

11   [3] Future Medicine Company Ltd., Seongnam, Gyeonggi-do 13449, Korea

12   #Address correspondence to Eric J. Snijder; E.J.Snijder@lumc.nl

13   * Present address: Netherlands Commission on Genetic Modification, Bilthoven, The Netherlands

14

15   **Running title:** Antiviral activity of DFA against coronaviruses

16   **Abstract:**   250 words

17   **Figures:**   5

18   **Tables:**   2

Abstract

The severe acute respiratory syndrome coronavirus 2 (SARS-CoV-2) pandemic has highlighted the lack of treatments to combat infections with human or (potentially) zoonotic CoVs. Thus, it is critical to develop and evaluate antiviral compounds that either directly target CoV functions or modulate host functions involved in viral replication. Here, we demonstrate that low-micromolar concentrations of 6',6'-difluoro-aristeromycin (DFA), an adenosine nucleoside analogue, strongly inhibit the replication of Middle East respiratory syndrome coronavirus (MERS-CoV) in a cell-based infection assay. DFA was designed to target S-adenosylhomocysteine (SAH) hydrolase and, consequently, may affect intracellular levels of the methyl donor S-adenosylmethionine, which is used by two CoV methyltransferases involved in the capping of the 5' end of the viral mRNAs. Passaging of wild-type MERS-CoV in the presence of DFA selected a mutant with a ~100-fold decreased DFA sensitivity. This drug-resistant population carried various amino acid substitutions in the viral nonstructural proteins (nsp), including mutations in nsp16, which has 2'-O-methyltransferase activity, and nsp13, which contains a nucleoside triphosphate hydrolase activity that has also been implicated in CoV capping. Based on our results, we hypothesize that DFA directly or indirectly affects viral cap methylation, either by inhibiting the viral enzymes involved or by binding to SAH hydrolase. We also evaluated the antiviral activity of DFA against other betacoronaviruses, but found it to have limited impact on their replication, while being quite cytotoxic to the Calu-3 cells used for this comparison. Nevertheless, our results justify the further characterization of DFA derivatives as an inhibitor of MERS-CoV replication.

Introduction

Previously, the emergence of severe acute respiratory syndrome coronavirus (SARS-CoV; in 2003 in China) and Middle East respiratory syndrome coronavirus (MERS-CoV; in 2012 in Saudi Arabia) highlighted the potential pandemic threat posed by this type of zoonotic pathogens and the need to develop rapid response options to contain them (1-4). Due to the severity of the diseases caused by SARS-CoV and MERS-CoV, and their potential for zoonotic transmission and global spread, both these agents received a priority status from the World Health Organization and other government agencies for the development of prophylactic and therapeutic treatment strategies (5, 6). The current SARS-CoV-2 pandemic (7, 8) and its burden on public health worldwide further emphasize the critical nature of the quest for anti-CoV drugs with high clinical efficacy. Thus far, only remdesivir was approved for emergency treatment of COVID-19 patients in the United States of America, Europe, and Japan. Many drug classes currently are under evaluation as inhibitors of CoV replication, including both compounds directly targeting viral functions, like viral proteases and the RNA polymerase, and host factor-targeting inhibitors (reviewed in (9-12)).

Coronaviruses are positive-stranded RNA (+RNA) viruses with a single genomic RNA of approximately 30 kb that is replicated in the cytoplasm of infected cells. Following entry, the 5'-capped viral genome is recognized and translated by host ribosomes to yield the replicase polyproteins pp1a and pp1ab (13). Subsequently, these large precursors are processed into 16 individual nonstructural proteins (nsp 1 to 16), which are released following polyprotein cleavage by two or three internal proteases. Together, the nsps form a multi-enzyme complex that ensures the replication of the viral genome and the transcription of a set of subgenomic mRNAs (reviewed in (14, 15)). The enzymatic core of this complex is formed by the nsp12 RNA-dependent RNA polymerase (RdRp) that synthesizes RNA with the help of the auxiliary factors nsp7 and nsp8 (16, 17), the nsp13 helicase that unwinds RNA duplexes (18-20), and several other RNA-processing enzymes residing in nsp12-nsp16 (reviewed in (15, 21, 22)). These also include a 3'-to-5' exoribonuclease (nsp14-ExoN) that is thought to increase replication fidelity by correcting mismatches sustained during RNA synthesis (reviewed in (23-26)). The viral structural and accessory proteins, encoded by smaller open reading frames located in the 3'-proximal part of the genome, are expressed from a set of 5'-capped and 3'-polyadenylated subgenomic mRNAs (reviewed in (15, 22)). Apart from ensuring mRNA recognition during formation of the ribosomal preinitiation complex, the 5'-terminal cap structure protects the viral mRNAs from degradation by cellular ribonucleases and prevents detection by the host's intracellular pathogen recognition receptors, which would trigger innate immune responses (reviewed in (27)).

69   The CoV capping mechanism is thought to consist of four sequential reactions: (i) an RNA triphosphatase

70   activity residing in nsp13 removes the γ-phosphate group from the 5'-triphosphorylated RNA (28, 29); (ii)

71   a guanosine monophosphate (GMP) is transferred to the 5'-diphosphate terminus by a yet to be confirmed

72   guanylyltransferase (GTase)(30), which was recently proposed to reside in the N-terminal nucleotidyl

73   transferase (NiRAN) domain of nsp12 (31); (iii) the nsp14 methyltransferase (MTase) methylates the cap's

74   5'-terminal guanine at the N7-position, producing the so-called cap-0 structure, ^{7me}GpppN (32); (iv) finally,

75   a cap-1 structure is formed when nsp16, in complex with its nsp10 co-factor, methylates the ribose 2'-O-

76   position of the first transcribed nucleotide of each viral RNA, converting ^{7me}GpppN into ^{7me}GpppN$_{2'me}$ (33).

77   Biochemical studies demonstrated that N7-methylation of the cap is a pre-requisite for its subsequent 2'-

78   O-methylation by nsp16/nsp10 (34-36). Given the central position of the RNA-synthesizing and capping

79   machinery in the CoV replication cycle, each single component constitutes a potential target for direct-

80   acting antiviral drug development.

81   As in cellular methylation reactions, S-adenosyl-L-methionine (SAM) is the most common methyl donor

82   used by viral MTases, such as those present in CoV nsp14 and nsp16 (37, 38). Thus, the identification of

83   compounds that can interfere with viral mRNA capping, by either directly targeting viral MTases or

84   indirectly affecting the concentrations of essential cellular metabolites, constitutes a viable strategy to

85   develop broad-spectrum CoV inhibitors. S-Adenosyl-homocysteine (SAH) is released upon the transfer of

86   the methyl group of SAM to a nucleic acid substrate by a SAM-dependent MTase. Consequently,

87   accumulation of SAH can interfere with SAM-dependent MTase function due to product inhibition (39).

88   Inhibitors targeting S-Adenosyl-homocysteine (SAH) hydrolase have been reported as potential broad-

89   spectrum antiviral drugs in different studies (40-42). This hydrolase catalyzes the reversible conversion of

90   SAH into adenosine and L-homocysteine, which both are then further metabolized for use in different

91   cellular pathways (43, 44).

92   Recently, using cell-based assays for MERS-CoV, SARS-CoV, chikungunya and Zika virus replication, we

93   described the inhibitory potential of a set of adenosine and selenoadenosine analogues (41). These

94   compounds were derived from aristeromycin, a well-known carbocyclic nucleoside compound that

95   inhibits SAH hydrolase and exhibits anti-viral, anti-cancer and anti-toxoplasma activities (reviewed in (45)).

96   These aristeromycin derivatives are nucleoside analogues designed to directly target viral RdRp activity

97   and/or indirectly target the methylation of viral RNA by inhibiting the host SAH hydrolase (41). From this

98   library, we identified 6',6'-difluoro-aristeromycin (DFA) as the aristeromycin derivative that inhibited

99   MERS-CoV replication most efficiently in cell-based assays (41). In different cell lines, DFA inhibited MERS-

100   CoV replication at low micromolar concentrations and could potently reduce the progeny titers produced

101   by MERS-CoV. Evaluation of the potential of DFA as a broad-spectrum antiviral compound revealed limited

102   inhibition of the replication of different β-CoVs at non-cytotoxic concentrations. This suggests that DFA-

103   based derivatives need to be developed to improve the antiviral activity of this compound class and reduce

104   the cytotoxic side- effects.

105

Results

107 <u>DFA inhibits MERS-CoV replication at low-micromolar concentrations in different cell lines</u>

108   DFA was part of a library of more than 80 adenosine and selenoadenosine analogues that was previously

109   evaluated for its antiviral activity against MERS-CoV, SARS-CoV and mouse hepatitis virus (MHV) using cell-

110   based cytopathic effect (CPE) reduction assays. From this analysis, DFA was identified as the most potent

111   inhibitor of MERS-CoV and SARS-CoV replication, with EC_{50} values (half-maximum effective concentration)

112   of 0.2 µM and 0.5 µM, respectively. The compound was found to be more effective in reducing the

113   progeny titers of MERS-CoV than those of SARS-CoV, yielding reductions of more than 3 $\log_{10}$ and 1 $\log_{10}$,

114   respectively, when treating Vero cells with 1.2 µM of DFA (41). We now evaluated the antiviral activity of

115   DFA against MERS-CoV in more detail using two independent cell-based assays: a CPE-reduction assay and

116   a dose response assay, using previously described protocols (46, 47).

117   Different cell lines of human (Huh7 and MRC-5) and non-human origin (Vero) were treated with increasing

118   concentrations of DFA and infected with MERS-CoV at a low multiplicity of infection (MOI) of 0.01.

119   Remdesivir (RDV) and chloroquine (CHO) were included as positive controls for inhibition of viral

120   replication. The mean EC_{50} values in Vero cells for these control compounds, RDV and CHO, were 0.4 µM

121   and 25 µM, respectively, similar to what was described previously (48, 49). Using CPE reduction assays,

122   EC_{50} values in the low-micromolar range were measured for DFA in each of the three cell lines: 0.2 µM in

123   Vero cells, 5.2 µM in Huh7 cells, and 2.3 µM in MRC-5 cells (Fig. 1A-C). In cytotoxicity control studies, the

124   corresponding CC_{50} values (the compound concentration resulting in 50% cytotoxicity) were calculated to

125   be 3.6 µM in Vero, 64 µM in Huh7, and >100 µM in MRC-5 cells (Fig 1A-C). Differences between cell lines

126   in sensitivity (cytotoxicity) to DFA treatment, as observed here, may reflect variation in SAH hydrolase

127   expression (a target of DFA) or uptake and metabolization of the compound.

128   In order to analyze the inhibitory effect of DFA on MERS-CoV progeny production in more detail, a

129   multiple-cycle dose response assay was performed. Cells were again infected at MOI 0.01, which was

130   followed by treatment with an increasing dose of DFA, ranging from 0.05 to 50 µM. Infected cell culture

131   supernatants were harvested at 48 h post infection (h p.i). and viral progeny titers were determined by

132   plaque assay in Vero cells. A dose-dependent reduction of viral progeny was observed, with a 4 to 5 $\log_{10}$

133   decrease following treatment with >1.2 µM of DFA in Vero cells, >2.4 µM in Huh7, and >12.5 µM in MRC-

134   5, respectively (Fig. 1D-F). Similar or lower EC_{50} values than in the CPE reduction assay were calculated

135   from these studies: 0.2 µM in Vero cells, ~0.8 µM in Huh7 cells, and 1.4 µM in MRC-5 cells. These results

136 indicated that DFA exhibits a similar antiviral activity across multiple cell lines resulting in a consistent ~3.5

137 to 4-log$_{10}$ reduction of MERS-CoV progeny titers.

138 Having established the strong inhibition of MERS-CoV replication by DFA, we also tested its

139 monophosphoramidate pro-drug (pDFA; Fig. 2A) in a CPE-reduction assay. This compound was

140 synthesized in order to circumvent the rate-limiting first phosphorylation step that presumably restricts

141 the efficient metabolization of nucleoside analogues like DFA following their uptake by the cell (reviewed

142 in (50)). Unfortunately, in this case the pro-drug was less active than DFA itself, independent of the cell

143 line used (Fig. 2B). Although the chemical and structural modifications of the prodrug decreased its

144 cytotoxicity, the calculated EC$_{50}$ values, 9 µM in Vero cells and 36 µM in MRC-5 cells, were more than 10

145 times higher than the ones measured for DFA (Fig. 1). Therefore, pDFA was not included in subsequent

146 experiments.

147

148 <u>DFA inhibits the early stage of MERS-CoV replication</u>

149 To characterize the mechanism of action of DFA in more detail, a time-of-addition assay was performed

150 to determine which stage of the viral replication cycle was inhibited by the compound. For this purpose,

151 Vero or MRC-5 cells were infected with MERS-CoV at high MOI (3 PFU/cell) and treated with DFA at

152 different time points pre and post infection at a concentration equaling 4 times the EC$_{50}$. We observed

153 inhibition of replication when the compound was administered before infection and at time points up to

154 4 h p.i. in Vero (Fig. 3A) and 8 h p.i. in MRC-5 (Fig. 3B). In Vero cells, a 2 log$_{10}$ reduction of progeny virus

155 titers was observed when the compound was administered between 24 h before infection and 1 h p.i. In

156 MRC-5 cells, DFA treatment led to a larger decrease of viral progeny production, >3 log$_{10}$, when treatment

157 was started up to 4 h p.i. At the DFA dosage used, no cytotoxicity was detected in either cell line (data not

158 shown). Replication kinetics of MERS-CoV is similar in Vero and MRC-5 cells (51, 52). Thus, the different

159 levels of progeny titer reduction observed between the two cell lines may be explained by variation in

160 uptake or metabolic conversion of the compound (53). In any case, these results demonstrated that DFA

161 inhibits an early stage of MERS-CoV replication.

162

163 <u>Selection of MERS-CoV mutants with 100-fold increased DFA resistance</u>

164 In order to explore the mode of action of DFA, we selected for compound-resistant MERS-CoV mutants.

165 For this purpose, wild-type MERS-CoV (wtP0) was serially passaged 10 times in MRC-5 cells in the presence

166   of increasing DFA concentrations (from 2.5 µM up to 45 µM). In each passage, two controls were taken

167   along: untreated cells infected with wt virus to monitor for cell culture adaptations (referred to as

168   'untreated wt'), and mock-infected cells treated with the corresponding concentration of DFA to assess

169   compound cytotoxicity. Development of CPE was monitored microscopically, and plaque phenotype and

170   viral progeny production were evaluated by plaque assay after each passage. From passage 8 (P8)

171   onwards, two of the three independently generated lineages showed no increased CPE compared to

172   uninfected, DFA-treated control cells, meaning that these virus populations could not replicate in the

173   presence of DFA concentrations above 35 µM, which were used in these later passages. When P8 virus

174   from lineages 1 or 2 was tested in a CPE-reduction assay, no increased DFA resistance was noticed

175   compared to an untreated wt virus control (data not shown). In contrast, lineage 3 (L3) virus did show

176   clear signs of developing DFA resistance. After 10 passages, infection of cells with L3P10 virus in the

177   presence of 45 µM DFA led to full CPE, which developed equally fast as for the untreated wt control. When

178   L3P10 virus was tested in a dose response assay, only a small (<0.5 $\log_{10}$) effect of DFA treatment on viral

179   progeny production was observed in the presence of up to 100 µM of DFA (Fig. 4A). When compared to

180   untreated wt (wtP10) or parental virus (wtP0), L3P10 virus displayed a more than 100-fold increased drug

181   resistance, with an EC_{50} value >100 µM against 0.8 µM for wtP10 and 0.4 µM for wtP0.

182   In order to assess if the increased DFA resistance of L3P10 affected its replication kinetics in comparison

183   to the wt control, multi-cycle infections of MRC-5 cells were performed. The two viruses showed similar

184   growth kinetics (Fig. 4B) with peak titers of 6.1×10^6 PFU/ml (wt) and 7.5×10^6 PFU/ml (L3P10) at 48 h p.i.

185   Taken together, the replication kinetics and strongly increased DFA resistance suggested that, during serial

186   passaging in the presence of DFA, the L3P10 virus population had acquired mutations that account for a

187   strongly increased resistance to the compound.

188

189   <u>Mutations in the L3P10 virus population implicate DFA in the inhibition of viral capping</u>

190   In order to identify mutations that contribute to DFA resistance, we sequenced the L3P10 virus population

191   by Illumina next-generation sequencing. Subsequently, sequencing reads were mapped to the reference

192   sequence of MERS-CoV strain EMC/2012 (NC_019843.3; (3)). Sequence variants constituting less than 10%

193   of the total population of viral reads were excluded from further analysis. The short read length (150

194   nucleotides) did not allow us to determine which mutations were combined in the same genome. A total

195   of 14 mutations was identified: five synonymous and nine non-synonymous mutations distributed across

196   genes encoding nine different viral proteins. Translationally silent mutations were considered unlikely to

197   be relevant for the phenotypic profile of L3P10 and disregarded for further analysis. As shown in Table 1,

198   the majority of the identified non-synonymous mutations were present in only part of the viral population

199   (in 37% to 55% of the total reads), suggesting a complex pattern of virus evolution with DFA resistance

200   possibly relying on (different) combinations of mutations. Only L3P10 mutations leading to amino acid

201   substitutions in the viral replicase (nsp1 to nsp16) were considered to possibly be associated with DFA

202   resistance, as accessory proteins like that encoded by ORF5 are not essential for viral replication in cell

203   culture ((54) and reviewed in (55)). The CoV spike protein is involved in receptor recognition and viral

204   entry (56) and therefore an unlikely target for inhibition by nucleoside analogues. A G12033 to A mutation

205   in the nsp7-coding region resulting in a D73N substitution was also identified in untreated wtP10 and

206   therefore concluded to result from cell culture adaptation. The remaining mutations that should be

207   considered mapped to nsps 1, 3, 12, 13 and 16 (Table 1).

208   As DFA is a nucleoside analog and was designed as a dual-target inhibitor of RdRps and (indirectly) MTases

209   (41), we were particularly interested in mutations identified in viral enzymes involved in RNA synthesis

210   and capping. Therefore, we considered four nonsynonymous substitutions most likely to contribute to the

211   observed DFA-resistance of the L3P10 virus population: Y218F in the nsp12-NiRAN domain, R22K and

212   R161H in the nsp13 ZBD-helicase subunit, and L156F in the nsp16 2'-O-MTase (Table 1). The latter

213   mutation was the only one of the four that was present throughout the L3P10 population. Recently, the

214   nsp12 NiRAN domain was proposed to function as the capping GTase (31), while nsp13 and nsp16 are

215   both thought to be involved in the CoV capping mechanism (see Introduction; reviewed in (30)).

216   Therefore, we hypothesize that DFA treatment affects the MERS-CoV capping mechanism and -

217   consequently – overall virus replication. However, as further optimization of this compound is needed to

218   improve its selectivity index, we did not perform follow-up experiments to elucidate its mode of action at

219   this stage.

220

221   Evaluation of DFA potential as a pan-coronaviral inhibitor

222   Taking into account the lack of antivirals against SARS-CoV-2 and the capacity of DFA to inhibit both SARS-

223   CoV and MERS-CoV replication, we decided to explore the potential of DFA as a broad-spectrum antiviral.

224   To this end, Calu-3 cells, a human lung cell line that supports MERS-CoV, SARS-CoV and SARS-CoV-2

225   replication (57, 58), were treated with increasing concentrations of DFA and infected with each of these

226   viruses in a dose response assay. By using the same cell line for each of these CoVs, differences in DFA up-

227   take or metabolic conversion to its triphosphate form were eliminated. The results showed a dose-

228   dependent decrease in the production of viral progeny for MERS-CoV (Fig. 5A) and SARS-CoV-2 (Fig. 5C)

229   that follows the cytotoxicity of the compound. At a DFA concentration of 3.2 µM, only a small reduction

230   of MERS-CoV and SARS-CoV-2 progeny was observed, 0.5 to 1log$_{10}$. Surprisingly, the antiviral activity of

231   DFA against MERS-CoV in Calu-3 cells was severely reduced when compared to results obtained in other

232   cell lines, including another human lung cell line MRC-5 (Fig. 1D-F). In the case of SARS-CoV infection, a

233   minor inhibitory effect was observed at concentrations that appeared to be somewhat cytotoxic (Fig. 5B

234   and 5D), contrary to what was demonstrated in Vero E6 cells ((41) and Table 2). Unfortunately, in Calu-3

235   cells cytotoxicity was detected at low compound concentrations (>6.2 µM) and the inhibitory effects

236   observed could thus be associated with an overall decrease in relative cell viability. This indicates that the

237   design of improved DFA derivatives is needed to decrease cytotoxicity and improve inhibitory potency.

238

Discussion

This study describes that treatment with low-micromolar concentrations of DFA exhibit a strong antiviral effect on MERS-CoV replication in cell culture-based infection models (Fig. 1). Time-of-addition assays indicated that DFA reduced MERS-CoV progeny production when cells were treated prior to, at the time of, or within 4 h after infection (Fig. 3), suggesting that DFA interferes with the early stage of replication. Propagation of MERS-CoV in the presence of DFA led to the selection of a virus population with strongly enhanced resistance to this compound (Fig. 4). Subsequent sequence analysis revealed a potentially complex pattern of resistance evolution, exhibiting multiple mutations that are present in only part of the virus population, including several that map to enzymes involved in viral RNA synthesis and mRNA capping (Table 1).

DFA was originally designed to target the host SAH hydrolase directly and was demonstrated to inhibit this enzyme *in vitro* with an IC_{50} (50% inhibitory concentration) of 1.06 μM (41). The compound is a carbocyclic adenosine analogue based on the parental inhibitor aristeromycin (59, 60), which was further modified by incorporation of a difluorine group at the 6' (top) position of its sugar ring ((41) and Fig. 2A). This modification improved the binding affinity of the compound for human SAH hydrolase and, consequently, the inhibition of its enzymatic activity.

Previous studies demonstrated that treatment of cells with high-affinity SAH hydrolase inhibitors, such as neplanocin A and aristeromycin, increases the intracellular SAH concentration, preventing the metabolic conversion of SAH to adenosine and L-homocysteine (reviewed in (61)). Therefore, SAH hydrolase inhibitors reduce or deplete the intracellular pools of homocysteine and adenosine, the latter being produced exclusively by SAH hydrolysis. As the SAM methyl donor is formed via homocysteine trans-sulfuration or the adenosine kinase pathway, SAH hydrolase regulates the intracellular SAM levels and consequently the cell's SAM-dependent methylation reactions. Moreover, SAH accumulation can also reduce the activity of SAM-dependent methyltransferases by feed-back inhibition, as SAH can bind to their active site with higher affinity than SAM itself (39). (62)

A correlation between the antiviral effect of adenosine analogues and their ability to interfere with viral capping has been demonstrated in previous studies with chikungunya virus, dengue virus, West Nile virus and vaccinia virus (63-66). Both CoV methyltransferases use SAM as a methyl donor for their enzymatic activity (36, 67, 68). Thus, SAH hydrolase inhibition and reduced SAM concentrations may impact, if not block, their activity. Previous studies with 5'-β-fluoroadenosine and derivatives of aristeromycin demonstrated that inhibition of SAH hydrolase affects viral replication by reducing RNA methylation

11

270 (reviewed in (61)). Moreover, neplanocin A, another SAH hydrolase inhibitor, was proven to bind to

271 methionine and prevent SAM production. Consequently, this leads to a block of 2'-O-methylation up to

272 60% (reviewed in (69)). Biochemical analysis of the MERS-CoV nsp16/nsp10 complex showed the capacity

273 of this enzyme to bind SAH with greater affinity than SAM (34), whereas superimposition of the SARS-CoV

274 nsp16/nsp10 in complex with SAH demonstrated that the same binding site is used by both substrates

275 (70). In addition, increased SAH concentrations reduced the 2'-O-methylation of N7-methylated

276 substrates (34, 68). In a similar manner, inhibition of the CoV capping pathway is a likely mode of action

277 (MoA) of DFA, although the genotypic profile of the L3P10 virus population does not exclude the possibility

278 that DFA may inhibit CoV replication using multiple mechanisms. As the identified mutations have not

279 been characterized in structural or biochemical studies, one can only speculate about their potential role

280 in viral replication and DFA resistance. However, it is striking that, with the exception of nsp1-D172H and

281 nsp3-R1314C, they all map to replicase subunits that have been implicated in viral capping: nsp12 (Y218F),

282 nsp13 (R22K and R161H) and nsp16 (L156F). The capping GTase role of the nsp12-NiRAN domain was (only

283 recently) proposed following structural and biochemical studies (31), and is still a matter of debate (71,

284 72). Based on the SARS-CoV-2 nsp12 structure, the identified Tyr to Phe change (Y218F in MERS-CoV) is

285 located in the proposed interaction interface with nsp9, next to two residues of nsp12 (D218 and R116 in

286 SARS-CoV-2) that form close contacts with the β-phosphate of the GDP, according to the recently acquired

287 cryo-EM structure of a mini-RTC (nsp7/nsp8/nsp9/nsp12/nsp13 complex) (73). The nsp13 mutations R22K

288 and R161H represent (semi)conservative replacements of residues in the N-terminal Cys/His-rich zinc-

289 binding domain (ZBD) and domain 1B of the helicase, respectively, according to the MERS-CoV nsp13

290 crystal structure (pdb 5WWP; (74)). These regions are known to be important for nsp13's interactions with

291 other RTC components and for protein flexibility (74, 75). In addition, helicase domain 1B constitutes the

292 RNA-binding channel. Molecular modeling of the MERS-CoV 2'-O-MTase places nsp16 residue L156 in

293 close proximity of the SAM-binding pocket of the nsp16/nsp10 complex bound to ^{7m}Gppp-RNA (34).

294 Although, we did not yet establish which of the mutations occur together in the same viral genome, the

295 presence of the L156F mutation in >99% of the NGS reads suggest that this substitution is essential for

296 DFA resistance and can possibly be supplemented with one of the other mutations in nsp12 and/or nsp13

297 (Table 1).

298 An additional passage of L3P10 in the presence of 45 μM of DFA (yielding L3P11) yielded a population with

299 a similar genetic profile albeit with an additional disruptive single-nucleotide insertion in ORF4. A similar

300 stable presence of multiple (potential) resistance mutations in part of the population has been observed

301 for viruses treated with mutagenic agents (76-78). Further phenotypical and mechanistic studies will be

12

302   needed to better understand the mode of action of DFA. Additionally, cloning of L3P10 viruses by plaque

303   picking could help to define the combination(s) of mutations that are the basis for DFA resistance, by

304   evaluating their frequency of occurrence and associated replication and plaque phenotype.

305   As a nucleoside analogue, DFA was considered to be a potential RdRp inhibitor. This would require uptake

306   by the cell's nucleoside transporters, and subsequent phosphorylation into a triphosphorylated product

307   that could be incorporated into the RNA chain during viral RNA synthesis (reviewed on (50)). In order to

308   improve absorption of the compound by the cells and metabolism into its active form, a prodrug of DFA

309   was synthesized and its antiviral activity was evaluated. In theory, the monophosphoramidate mask would

310   promote the second phosphorylation to occur once the compound enters the cytoplasm by circumventing

311   the rate-limiting step of the first phosphorylation. However, when compared to DFA, the EC_{50} of the

312   prodrug was more than 10 times higher (Fig. 2), in contrast to results obtained with prodrugs of other

313   nucleoside analogues (49, 79). In previous work, structure-activity studies and tests of several purine and

314   pyrimidine analogues of DFA suggested that DFA is most likely not targeting the RdRp (41, 65, 80). This

315   notion is also supported by the fact that the genotypic profile obtained for L3P10 did not reveal mutations

316   in the RdRp domain of nsp12.

317   Currently, there is a lack of antiviral drugs with proven efficacy against human CoV infections, including

318   the MERS-CoV that is endemic in the Middle East, the current pandemic SARS-CoV-2 and potential future

319   zoonotic CoV. This highlights the importance to investigate new drug targets and identify antiviral

320   compounds with potential broad-spectrum activity against CoVs. Previous reports demonstrated that SAH

321   hydrolase inhibitors are active against different DNA viruses (in particular poxviruses), double-stranded

322   RNA viruses (reoviruses), (–)RNA viruses (bunya-, arena-, rhabdo-, filo-, ortho- and paramyxoviruses) and

323   (+)RNA viruses like alpha- and flaviviruses (64, 65, 81-85). This type of compounds, that mainly targets

324   cellular proteins, usually exhibits a broader antiviral spectrum, but has a higher likelihood of being toxic.

325   The cell-dependent antiviral activity of DFA against MERS-CoV emphasizes the importance of comparing

326   different cell lines when testing compounds that can target cellular factors. In this study, we demonstrate

327   that DFA can inhibit the replication of MERS-CoV, but that the design and development of DFA-based

328   derivatives will be required to reduce cytotoxic side effects. Combining our results in this study with our

329   previous report (41), showing that DFA can inhibit chikungunya and Zika virus, DFA appears to be an

330   interesting compound for further development as a broad-spectrum antiviral agent.

331

Materials and Methods

Cell culture and viruses

Vero cells were a kind gift from the Department of Viroscience, Erasmus Medical Center, Rotterdam, the Netherlands, and Huh7 cells were provided by Dr. Ralf Bartenschlager, Heidelberg University, Germany. Vero, Huh7 and Baby hamster kidney cells (BHK-21; ATCC CCL10) were cultured as described before (51, 86, 87). MRC-5 cells (ATCC CCL-171) were maintained in Eagle's minimum essential medium (EMEM; Lonza) supplemented with non-essential amino acids (PAA), 8% fetal calf serum (FCS; Bodinco), 100 units/ml penicillin (Lonza), 100 units/ml streptomycin (Lonza) and 2 mM L-glutamine (PAA). Calu-3 cells (ATCC HTB-55) were cultured in EMEM medium complemented with 10% FCS, penicillin/streptomycin, 2 mM L-glutamine, non-essential amino acids and sodium pyruvate (Life technologies). All cells were incubated at 37°C with 5% CO_2. Infections were carried out in EMEM containing 25 mM HEPES (Lonza), 2% FCS, penicillin/streptomycin and L-glutamine (nominated from now on as EMEM-2%FCS). MERS-CoV (strain EMC/2012; (3, 4)), SARS-CoV (Frankfurt-1 strain,(88)), SARS-CoV-2/Leiden-0002 (GenBank accession nr. MT510999; (89)), MHV (strain A59; (90)) and EAV (Bucyrus isolate; (91)) were used for infections with wild type virus. Human CoV infections were performed inside biosafety cabinets in a certified biosafety level 3 (BSL3) facilities at Leiden University Medical Center.

Compounds

6',6'-Difluoro-aristeromycin (DFA) and its adenine phosphoramidate pro-drug (pDFA) were designed and synthesized, designated as 2c and 3a, respectively, as described in a previous report (41). Different batches of powder were dissolved in DMSO to a final concentration of 20 mM and single use aliquots were stored at 4°C. Remdesivir (RDV; HY-104077) was purchased from MedChemexpress and chloroquine (C6628) from Sigma. Both compounds were dissolved in adequate solvents (DMSO or PBS, respectively) and single use aliquots were stored at -20°C.

Cytopathic effect (CPE) reduction assay

Cells were seeded in 96-well flat bottom plates in 100 µl at a density of 10000 cells/well of Huh7, 15000 cells/well of MRC-5 or 20000 cells/well of Vero cells. After overnight culture at 37°C, cells were pre-incubated for 30 min with 50 µl of two-fold serial dilutions of compounds prepared in EMEM-2%FCS. Subsequently, half of the wells were infected with MERS-CoV at low MOI in a total volume of 150 µl of

14

362 medium with increasing concentrations between 0.05 to 100 uM compound, to evaluate the inhibitory

363 effect of compound. The other half of the wells were "mock"-infected with medium to monitor the

364 (potential) cytotoxicity of the compound. Plates were incubated for three days at 37°C, after which cell

365 viability was measured using the colorimetric CellTiter 96® Aqueous Non-Radioactive Cell Proliferation kit

366 (Promega). The absorption at 495 nm was measured using a monochromatic filter in a multimode plate

367 reader (Envision; Perkin Elmer). Data were normalized to the "mock"-infected control, after which EC_{50}

368 and CC_{50} values were calculated using non-linear regression with Graph-Pad Prism V8.0. Each experiment

369 was performed at least in quadruplicate and repeated at least twice.

370

371 <u>Dose response assay</u>

372 To evaluate the effect of compound treatment on viral progeny titers, confluent monolayers of Vero, Huh7

373 or MRC-5 were seeded in 24-well plates. Cells were incubated for 30 min at 37°C with solvent or a range

374 of LJ-4269 concentrations (from 0.1 to 100 uM). Then, cells were infected with MERS-CoV at an MOI of

375 0.01 for 1 h. After infection, cells were washed three times with PBS and 1 ml of medium with compound

376 was added. Supernatants were collected at 48 h p.i. and viral progeny titers were determined by plaque

377 assay in Vero cells as described before (92).

378 In 96-well clusters, Calu-3 cells were seeded at a density of 3×10^4 cells per well in 100 µl culture medium.

379 Two days later, cells were pre-incubated for 30 min with 2-fold serial dilutions of compound, starting at a

380 concentration of 25 µM. Subsequently, cells were infected with MERS-CoV, SARS-CoV or SARS-CoV-2 (MOI

381 of 1 based on titer determined on Vero cells) in the presence of compound for 1 h. Next, cells were washed

382 three times with PBS and 100 µl of compound solution in EMEM-2%FCS was added. Supernatants were

383 collected at 24 h p.i. and progeny virus titers were determined by plaque assay.

384

385 <u>Time of addition assay</u>

386 Confluent monolayers of MRC-5 or Vero cells were seeded in 12-well plates in 1 ml/well of the appropriate

387 medium (see above), and were grown overnight at 37°C. Treatment of cells (before, during or after

388 infection) was performed using 0.6 µM (for Vero) and 12.5 µM (for MRC-5) of compound solution freshly

389 prepared in EMEM-2%FCS medium. Cells were infected with MERS-CoV inoculum (MOI of 5) for 1h and

390 washed three times with PBS. Subsequently, EMEM-2%FCS medium was added to the cells and

391   supplemented with compound solution in 2-h intervals to a final concentration as mentioned above.

392   Supernatants were collected 16 h p.i. and viral titers were determined by plaque assay.

393

394   <u>Resistance culturing and next-generation sequencing (NGS)</u>

395   Recombinant wt MERS-CoV strain EMC/2012(rMERS-CoV) was passaged in triplicate in presence of

396   increasing concentrations of DFA ranging from 3.2 µM to 45 µM. Infections were performed at an MOI of

397   0.05 in every passage in MRC-5 monolayers. In parallel, rMERS-CoV wt was passaged in the same

398   conditions in the absence of compound, to identify possible mutations associated with cell culture

399   adaptation. Additionally, a "mock"-infected well treated with the same concentration of compound in

400   each passage was evaluated for cytotoxicity by light microcopy. Supernatants were harvested when 80%

401   to full CPE was observed (usually at 3 d p.i.). Three lineages were generated by serial passaging, but only

402   lineage 3 was used for next-generation sequencing. To this end, RNA was isolated from 200 µl of virus-

403   containing cell culture supernatants using TriPure isolation reagent (Roche Applied Science) and purified

404   according to manufacturer's instructions. The RNA concentration was measured using a Qubit

405   fluorometer and RNA High Sensitivity kit (Thermo Fisher Scientific). NGS sample preparation and analysis

406   were performed as described previously (93). After filtration and trimming of data, the remaining reads

407   were mapped to the MERS-CoV GenBank reference sequence (NC_019843;(3)). Changes (mutation,

408   deletions and insertions) were considered relevant when constituting more than 10% of the total

409   population of viral reads (Table 1)(4). Raw NGS data set for L3P10 sample analysed in this study is

410   deposited in NCBI Bioproject and available under the following link:

411   http://www.ncbi.nlm.nih.gov/bioproject/730836. Only MERS-CoV-specific reads were included in

412   these data files.

413

414   **Acknowledgments**

418

419   **Figures**
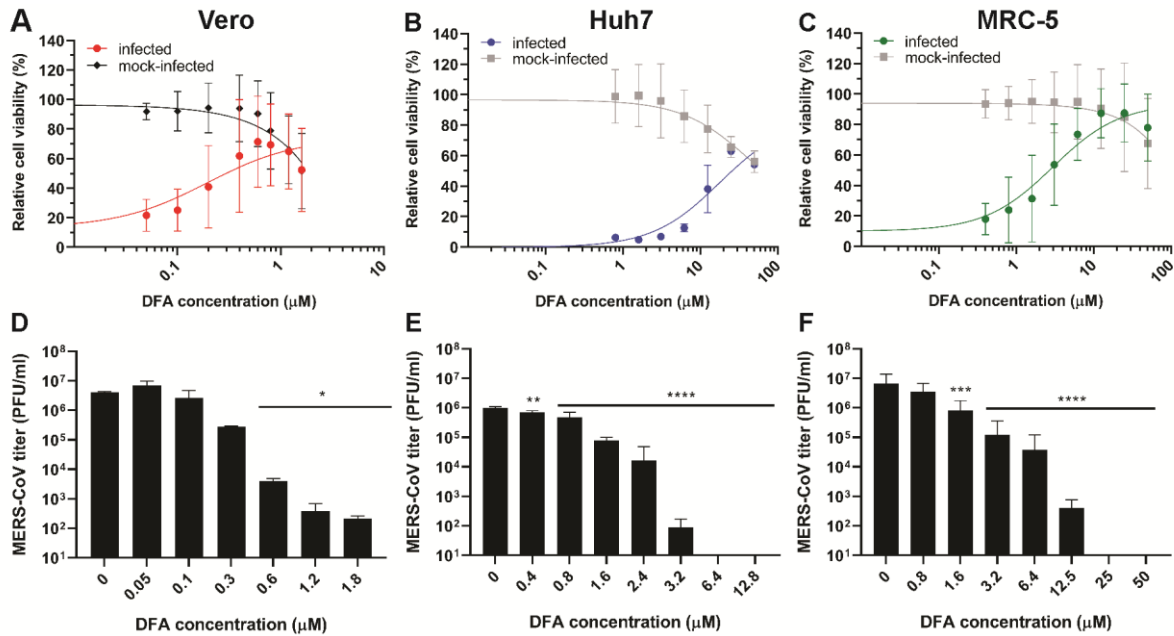
Figure 1- DFA inhibits MERS-CoV replication in different cell lines. Vero (A and D), Huh7 (B and E) and MRC-5 (C and F) were treated with a two-fold dilution series of DFA in the low-micromolar range and infected with MERS-CoV. Inhibitory effect was evaluated by a CPE-reduction assay (A-C) or dose response assay (D-F). For the CPE-reduction assay, cell viability was assayed using the CellTiter 96 Aqueous One Solution cell proliferation assay (MTS assay) 3 d p.i.. The graphs show the results of at least two independent experiments (mean ± sd are shown). A non-linear regression analysis was applied. In the dose response assay, cell supernatants were collected after 2 d.p.i and viral progeny was titrated by plaque assay on Vero cells. Error bars represent standard deviation. Statistical significance was determined by one-way ANOVA. *, $p < 0.1$; **, $p < 0.01$; ***, $p < 0.001$; ****, $p < 0.0001$.

420
421

17
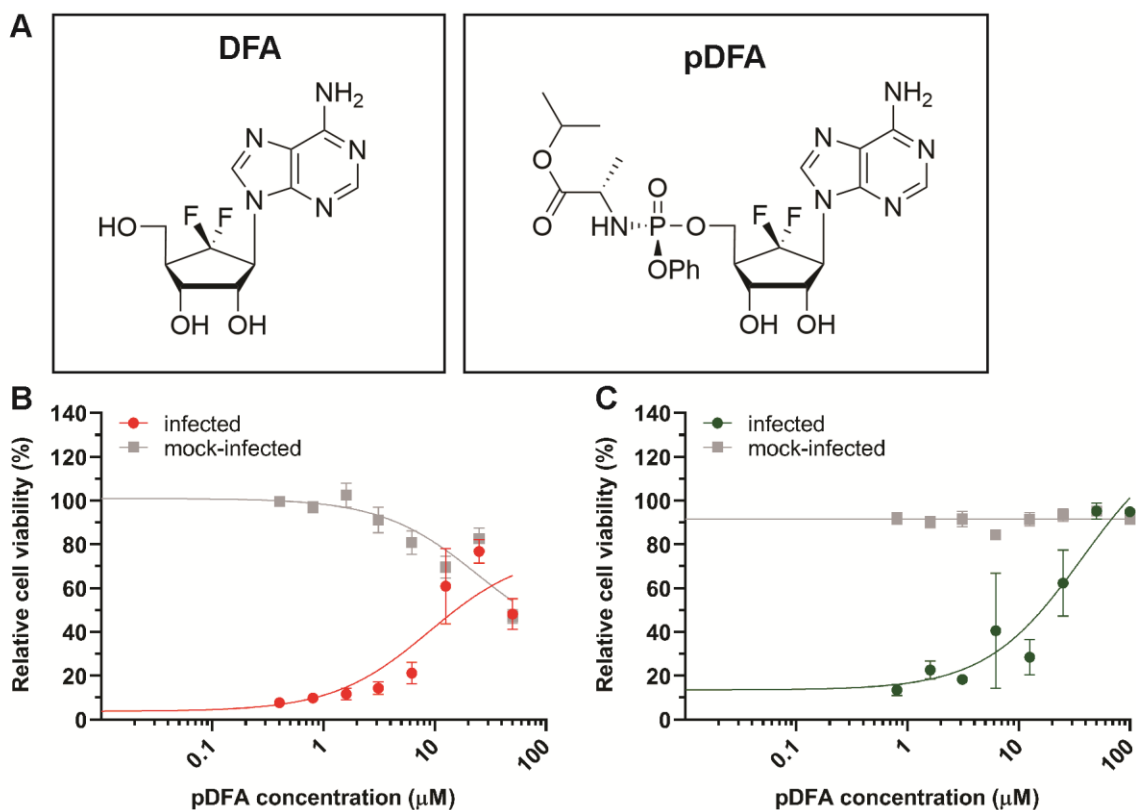
Figure 2- DFA prodrug inhibits MERS-CoV replication. (A) DFA and pDFA schematic structure. pDFA antiviral activity was evaluated by a CPE-reduction assay. (B) Vero or (C) MRC-5 cells were treated with two-fold serial dilution of pDFA and infected with MERS-CoV. After 3 d p.i., cell viability was measured using the CellTiter 96 Aqueous One Solution cell proliferation assay (MTS assay). The graphs show the results of two independent experiments (mean ± sd are shown). A non-linear regression analysis was applied.

422
423

Figure 3- DFA inhibits early steps of MERS-CoV replication. Vero (A) and MRC-5 (B) cells were treated with 0.6 and 12.5 μM, respectively, at the indicated time points pre- and post-infection. Viral progeny in supernatant harvested at 16 h p.i. was determined by plaque assay in Vero cells. The data represent the results from duplicates of 2 independent experiments. Error bars represent standard deviations. Statistical significance was determined by one-way ANOVA.; *, $p<0.1$; **, $p<0.01$; ***, $p<0.001$; ****, $p<0.0001$.
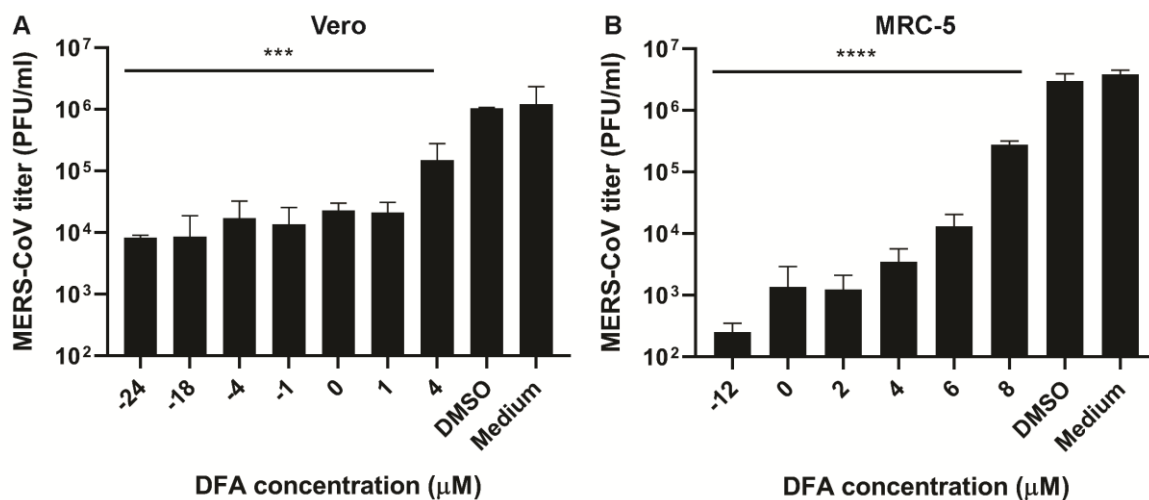
424
425

19
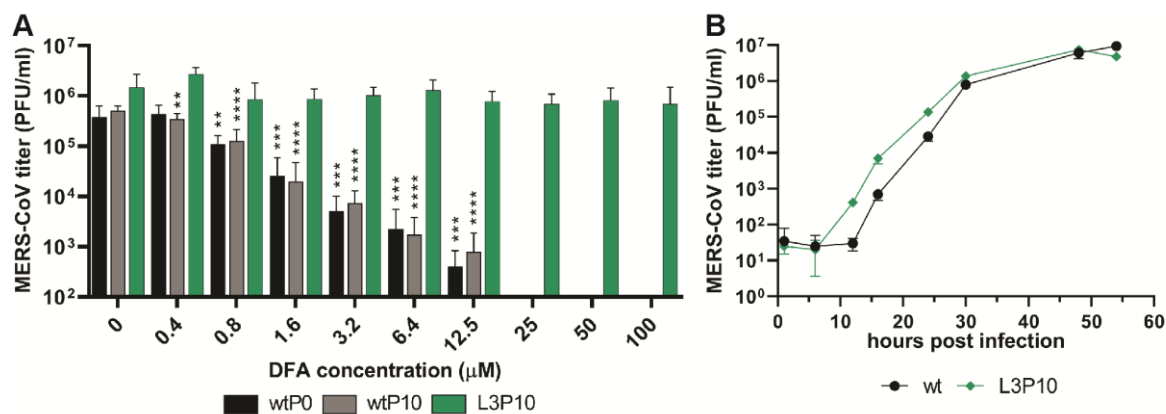
Figure 4- Resistant MERS-CoV mutants selected by passaging in the presence of DFA. Replication in MRC-5 cells of a DFA-resistant virus population (L3P10) in the presence of increasing concentrations of DFA, compared to the parental virus (wtP0) and untreated wt virus (wtP10). Cells were infected with MOI 0.01 and virus progeny in supernatant harvested at 48 h p.i. The data represent the results from four replicates obtained in 2 independent experiments. (B) Characterization of growth kinetics of selected resistant mutant (L3P10). MRC-5 cells were infected with MOI 0.01 and supernatants were harvested at indicated time points from triplicate wells. Viral progeny titers were determined by plaque assay in Vero cells (mean ± sd is presented). Statistical significance was determined by one-way ANOVA. *, $p<0.1$; **, $p<0.01$; ***, $p<0.001$; ****, $p<0.0001$.

426
427
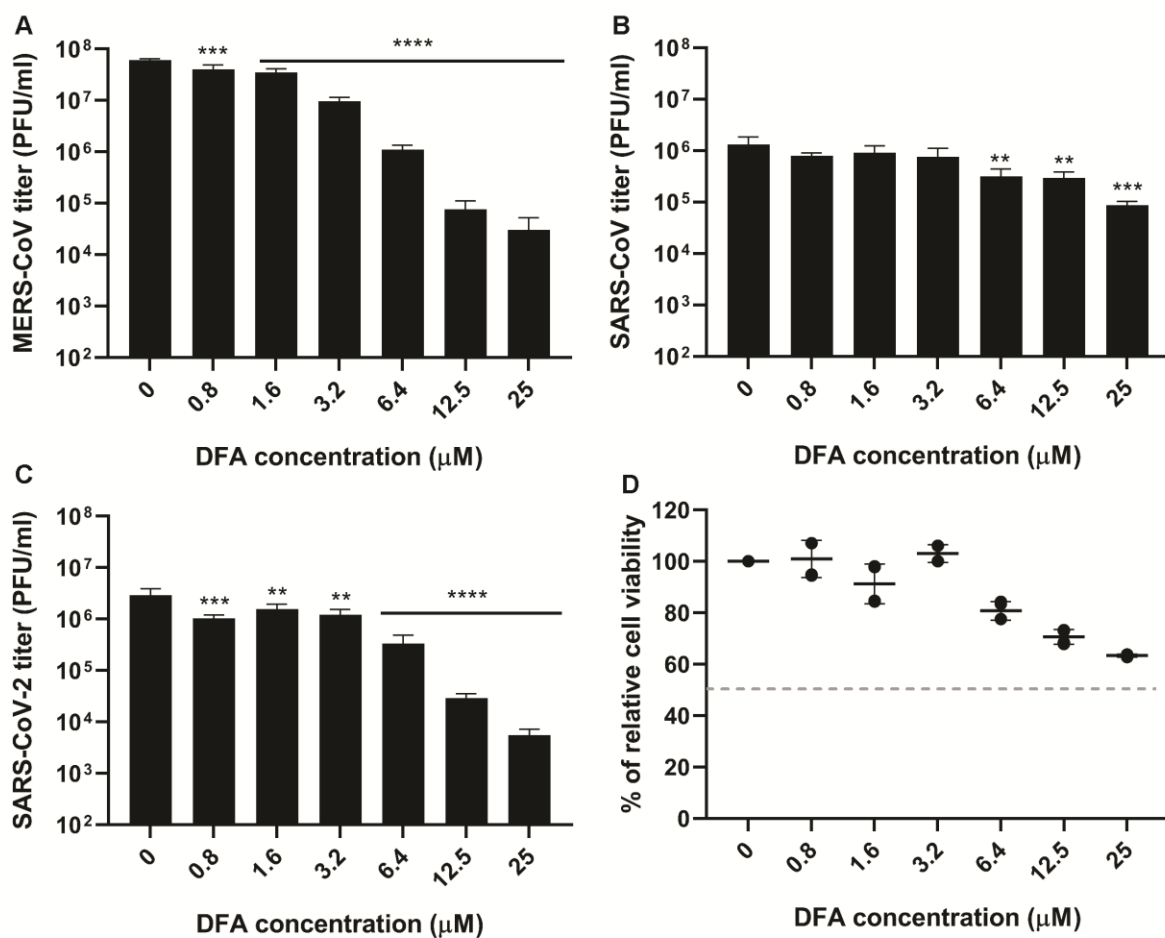
Figure 5- DFA antiviral activity is reduced in Calu-3 cells. Calu-3 cells were infected with MERS-CoV (A), SARS-CoV (B) and SARS-CoV-2 (C) in the presence of various concentrations of DFA. An MOI of 1 was used, based on titrations of virus stocks on Vero cells. Progeny virus titers in supernatants harvested at 24 h p.i. were determined by plaque assay in Vero cells. (D) Cytotoxicity of DFA was measured in mock-infected cells, and was determined at 24 h p.i. in a CPE-reduction assay by use of the CellTiter 96 Aqueous One Solution cell proliferation assay (MTS assay). The data represent triplicates of 2 independent experiments and error bars show standard deviations. Statistical significance was determined by one-way ANOVA. No*, no significance; *, $p < 0.1$; **, $p < 0.01$; ***, $p < 0.001$; ****, $p < 0.0001$.

428

429

Table 1- Summary of non-synonymous mutations identified in MERS-CoV L3P10 by NGS

Coding region	nt change	aa change	Domain	Presence in L3P10 (NGS)
nsp1	G795C	D172H	CTD	55%
nsp3	C6777T	R1314C	PLnc	37%
nsp7	G12033A*	D73N		>99%
nsp12	A14061T	Y218F	NiRAN	48%
nsp13	G16272A	R22K	ZBD	49%
	G16689A	R161H	1B	40%
nsp16	C21068T	L156F	2'-O-MTase	>99%
spike	T24085_24086*ins*ACTCAACAGGTG	P876_V877ins TQQV		37%
ORF5	G26927_26928*ins*T	Not in frame		48%

nt, nucleotide; aa, amino acid; CTD, C-terminal domain; PLnc, papain-like noncanonical domain; NiRAN, Nidovirus RdRp associated nucleotidyl transferase domain; ZBD, Zinc binding domain; 1B, 1B domain of helicase; * also present in wtP10 control

430

Table 2 – The antiviral effect of DFA on the replication of different β-CoVs.

Virus	Cell line	EC_{50} (µM)	CC_{50} (µM)	SI
MERS-CoV	Vero	0.2	>3.2	>16
	HuH7	0.6	>50	>80
	MRC-5	0.8	>50	>60
	Calu-3	~2	>25	>12
SARS-CoV	Calu-3	~5	>25	>5
SARS-CoV-2	Calu-3	~2	>25	>12

EC_{50}s values were calculated based on results obtained in dose response assay, while CC_{50}s values were determined in a cell viability assay as described in materials and methods. SI, selectivity index was calculated by comparing CC_{50} with EC_{50} values.

431

23

References

1. Ksiazek TG, Erdman D, Goldsmith CS, Zaki SR, Peret T, Emery S, Tong S, Urbani C, Comer JA, Lim W, Rollin PE, Dowell SF, Ling AE, Humphrey CD, Shieh WJ, Guarner J, Paddock CD, Rota P, Fields B, DeRisi J, Yang JY, Cox N, Hughes JM, LeDuc JW, Bellini WJ, Anderson LJ, Group SW. 2003. A novel coronavirus associated with severe acute respiratory syndrome. N Engl J Med 348:1953-66.

2. Peiris JS, Lai ST, Poon LL, Guan Y, Yam LY, Lim W, Nicholls J, Yee WK, Yan WW, Cheung MT, Cheng VC, Chan KH, Tsang DN, Yung RW, Ng TK, Yuen KY, group Ss. 2003. Coronavirus as a possible cause of severe acute respiratory syndrome. Lancet 361:1319-25.

3. Zaki AM, van Boheemen S, Bestebroer TM, Osterhaus AD, Fouchier RA. 2012. Isolation of a novel coronavirus from a man with pneumonia in Saudi Arabia. N Engl J Med 367:1814-1820.

4. van Boheemen S, de Graaf M, Lauber C, Bestebroer TM, Raj VS, Zaki AM, Osterhaus AD, Haagmans BL, Gorbalenya AE, Snijder EJ, Fouchier RA. 2012. Genomic characterization of a newly discovered coronavirus associated with acute respiratory distress syndrome in humans. MBio 3:e00473-12.

5. Brende B, Farrar J, Gashumba D, Moedas C, Mundel T, Shiozaki Y, Vardhan H, Wanka J, Rottingen JA. 2017. CEPI-a new global R&D organisation for epidemic preparedness and response. Lancet 389:233-235.

6. Mehand MS, Al-Shorbaji F, Millett P, Murgue B. 2018. The WHO R&D Blueprint: 2018 review of emerging infectious diseases requiring urgent research and development efforts. Antiviral Res 159:63-67.

7. Zhou P, Yang XL, Wang XG, Hu B, Zhang L, Zhang W, Si HR, Zhu Y, Li B, Huang CL, Chen HD, Chen J, Luo Y, Guo H, Jiang RD, Liu MQ, Chen Y, Shen XR, Wang X, Zheng XS, Zhao K, Chen QJ, Deng F, Liu LL, Yan B, Zhan FX, Wang YY, Xiao GF, Shi ZL. 2020. A pneumonia outbreak associated with a new coronavirus of probable bat origin. Nature 579:270-273.

8. Munster VJ, Koopmans M, van Doremalen N, van Riel D, de Wit E. 2020. A novel coronavirus emerging in China - key questions for impact assessment. N Engl J Med 382:692-694.

9. Zumla A, Chan JF, Azhar EI, Hui DS, Yuen KY. 2016. Coronaviruses - drug discovery and therapeutic options. Nat Rev Drug Discov 15:327-47.

10. Garcia-Serradilla M, Risco C, Pacheco B. 2019. Drug repurposing for new, efficient, broad spectrum antivirals. Virus Res 264:22-31.

11. Dittmar M, Lee JS, Whig K, Segrist E, Li M, Jurado K, Samby K, Ramage H, Schultz D, Cherry S. 2020. Drug repurposing screens reveal FDA approved drugs active against SARS-Cov-2. bioRxiv doi:10.1101/2020.06.19.161042:2020.06.19.161042.

12. Valle C, Martin B, Touret F, Shannon A, Canard B, Guillemot JC, Coutard B, Decroly E. 2020. Drugs against SARS-CoV-2: What do we know about their mode of action? Rev Med Virol 30:1-10.

13. Snijder EJ, Bredenbeek PJ, Dobbe JC, Thiel V, Ziebuhr J, Poon LL, Guan Y, Rozanov M, Spaan WJ, Gorbalenya AE. 2003. Unique and conserved features of genome and proteome of SARS-coronavirus, an early split-off from the coronavirus group 2 lineage. J Mol Biol 331:991-1004.

477 14. Fehr AR, Perlman S. 2015. Coronaviruses: an overview of their replication and
478   pathogenesis. Methods Mol Biol 1282:1-23.
479 15. V'Kovski P, Kratzel A, Steiner S, Stalder H, Thiel V. 2020. Coronavirus biology and
480   replication: implications for SARS-CoV-2. Nat Rev Microbiol doi:10.1038/s41579-020-
481   00468-6.
482 16. Subissi L, Posthuma CC, Collet A, Zevenhoven-Dobbe JC, Gorbalenya AE, Decroly E,
483   Snijder EJ, Canard B, Imbert I. 2014. One severe acute respiratory syndrome coronavirus
484   protein complex integrates processive RNA polymerase and exonuclease activities. Proc
485   Natl Acad Sci U S A 111:E3900-E3909.
486 17. Kirchdoerfer RN, Ward AB. 2019. Structure of the SARS-CoV nsp12 polymerase bound
487   to nsp7 and nsp8 co-factors. Nat Commun 10:2342.
488 18. Seybert A, Hegyi A, Siddell SG, Ziebuhr J. 2000. The human coronavirus 229E
489   superfamily 1 helicase has RNA and DNA duplex-unwinding activities with 5'-to-3'
490   polarity. RNA 6:1056-68.
491 19. Adedeji AO, Singh K, Calcaterra NE, DeDiego ML, Enjuanes L, Weiss S, Sarafianos SG.
492   2012. Severe acute respiratory syndrome coronavirus replication inhibitor that interferes
493   with the nucleic acid unwinding of the viral helicase. Antimicrob Agents Chemother
494   56:4718-28.
495 20. Chen J, Malone B, Llewellyn E, Grasso M, Shelton PMM, Olinares PDB, Maruthi K,
496   Eng ET, Vatandaslar H, Chait BT, Kapoor TM, Darst SA, Campbell EA. 2020. Structural
497   Basis for Helicase-Polymerase Coupling in the SARS-CoV-2 Replication-Transcription
498   Complex. Cell 182:1560-1573 e13.
499 21. Posthuma CC, Te Velthuis AJW, Snijder EJ. 2017. Nidovirus RNA polymerases:
500   Complex enzymes handling exceptional RNA genomes. Virus Res 234:58-73.
501 22. Snijder EJ, Decroly E, Ziebuhr J. 2016. The Nonstructural Proteins Directing
502   Coronavirus RNA Synthesis and Processing. Adv Virus Res 96:59-126.
503 23. Ulferts R, Ziebuhr J. 2011. Nidovirus ribonucleases: Structures and functions in viral
504   replication. RNA Biol 8:295-304.
505 24. Denison MR, Graham RL, Donaldson EF, Eckerle LD, Baric RS. 2011. Coronaviruses:
506   an RNA proofreading machine regulates replication fidelity and diversity. RNA Biol
507   8:270-9.
508 25. Ogando NS, Ferron F, Decroly E, Canard B, Posthuma CC, Snijder EJ. 2019. The curious
509   case of the nidovirus exoribonuclease: its role in RNA synthesis and replication fidelity.
510   Front Microbiol 10:1813.
511 26. Robson F, Khan KS, Le TK, Paris C, Demirbag S, Barfuss P, Rocchi P, Ng WL. 2020.
512   Coronavirus RNA Proofreading: Molecular Basis and Therapeutic Targeting. Mol Cell
513   79:710-727.
514 27. Kindler E, Thiel V. 2014. To sense or not to sense viral RNA--essentials of coronavirus
515   innate immune evasion. Curr Opin Microbiol 20:69-75.
516 28. Ivanov KA, Thiel V, Dobbe JC, van der Meer Y, Snijder EJ, Ziebuhr J. 2004. Multiple
517   enzymatic activities associated with severe acute respiratory syndrome coronavirus
518   helicase. J Virol 78:5619-32.
519 29. Ivanov KA, Ziebuhr J. 2004. Human coronavirus 229E nonstructural protein 13:
520   characterization of duplex-unwinding, nucleoside triphosphatase, and RNA 5'-
521   triphosphatase activities. J Virol 78:7833-8.
522 30. Decroly E, Ferron F, Lescar J, Canard B. 2011. Conventional and unconventional
523   mechanisms for capping viral mRNA. Nat Rev Microbiol 10:51-65.

524 31. Yan L, Ge J, Zheng L, Zhang Y, Gao Y, Wang T, Huang Y, Yang Y, Gao S, Li M, Liu Z,
525   Wang H, Li Y, Chen Y, Guddat LW, Wang Q, Rao Z, Lou Z. 2020. Cryo-EM Structure
526   of an Extended SARS-CoV-2 Replication and Transcription Complex Reveals an
527   Intermediate State in Cap Synthesis. Cell doi:10.1016/j.cell.2020.11.016.
528 32. Chen Y, Cai H, Pan J, Xiang N, Tien P, Ahola T, Guo D. 2009. Functional screen reveals
529   SARS coronavirus nonstructural protein nsp14 as a novel cap N7 methyltransferase. Proc
530   Natl Acad Sci U S A 106:3484-3489.
531 33. Decroly E, Imbert I, Coutard B, Bouvet M, Selisko B, Alvarez K, Gorbalenya AE,
532   Snijder EJ, Canard B. 2008. Coronavirus nonstructural protein 16 is a cap-0 binding
533   enzyme possessing (nucleoside-2'O)-methyltransferase activity. J Virol 82:8071-84.
534 34. Aouadi W, Blanjoie A, Vasseur JJ, Debart F, Canard B, Decroly E. 2017. Binding of the
535   Methyl Donor S-Adenosyl-l-Methionine to Middle East Respiratory Syndrome
536   Coronavirus 2'-O-Methyltransferase nsp16 Promotes Recruitment of the Allosteric
537   Activator nsp10. J Virol 91.
538 35. Bouvet M, Lugari A, Posthuma CC, Zevenhoven JC, Bernard S, Betzi S, Imbert I, Canard
539   B, Guillemot JC, Lecine P, Pfefferle S, Drosten C, Snijder EJ, Decroly E, Morelli X.
540   2014. Coronavirus Nsp10, a critical co-factor for activation of multiple replicative
541   enzymes. J Biol Chem 289:25783-25796.
542 36. Bouvet M, Debarnot C, Imbert I, Selisko B, Snijder EJ, Canard B, Decroly E. 2010. In
543   vitro reconstitution of SARS-coronavirus mRNA cap methylation. PLoS Pathog
544   6:e1000863.
545 37. Lu SC. 2000. S-Adenosylmethionine. Int J Biochem Cell Biol 32:391-5.
546 38. Struck AW, Thompson ML, Wong LS, Micklefield J. 2012. S-adenosyl-methionine-
547   dependent methyltransferases: highly versatile enzymes in biocatalysis, biosynthesis and
548   other biotechnological applications. Chembiochem 13:2642-55.
549 39. Kloor D, Osswald H. 2004. S-Adenosylhomocysteine hydrolase as a target for
550   intracellular adenosine action. Trends Pharmacol Sci 25:294-7.
551 40. De Clercq E. 2002. Strategies in the design of antiviral drugs. Nat Rev Drug Discov 1:13-
552   25.
553 41. Yoon JS, Kim G, Jarhad DB, Kim HR, Shin YS, Qu S, Sahu PK, Kim HO, Lee HW,
554   Wang SB, Kong YJ, Chang TS, Ogando NS, Kovacikova K, Snijder EJ, Posthuma CC,
555   van Hemert MJ, Jeong LS. 2019. Design, Synthesis, and Anti-RNA Virus Activity of 6'-
556   Fluorinated-Aristeromycin Analogues. J Med Chem doi:10.1021/acs.jmedchem.9b00781.
557 42. Chen Q, Schneller SW, Liu C, Jones KL, Singer T. 2020. 5'-Nor-3-Deaza-1',6'-
558   Isoneplanocin, the Synthesis and Antiviral Study. Molecules 25.
559 43. Cantoni GL. 1975. Biological methylation: selected aspects. Annu Rev Biochem 44:435-
560   51.
561 44. Palmer JL, Abeles RH. 1979. The mechanism of action of S-adenosylhomocysteinase. J
562   Biol Chem 254:1217-26.
563 45. Rawal RK, Bariwal J, Singh V. 2016. Chemistry and Bioactivities of Aristeromycins: An
564   Overview. Curr Top Med Chem 16:3258-3273.
565 46. de Wilde AH, Raj VS, Oudshoorn D, Bestebroer TM, van Nieuwkoop S, Limpens RW,
566   Posthuma CC, van der Meer Y, Barcena M, Haagmans BL, Snijder EJ, van den Hoogen
567   BG. 2013. MERS-coronavirus replication induces severe in vitro cytopathology and is
568   strongly inhibited by cyclosporin A or interferon-alpha treatment. J Gen Virol 94:1749-
569   60.

570 47. de Wilde AH, Falzarano D, Zevenhoven-Dobbe JC, Beugeling C, Fett C, Martellaro C,
571   Posthuma CC, Feldmann H, Perlman S, Snijder EJ. 2017. Alisporivir inhibits MERS- and
572   SARS-coronavirus replication in cell culture, but not SARS-coronavirus infection in a
573   mouse model. Virus Res 228:7-13.
574 48. de Wilde AH, Jochmans D, Posthuma CC, Zevenhoven-Dobbe JC, van Nieuwkoop S,
575   Bestebroer TM, van den Hoogen BG, Neyts J, Snijder EJ. 2014. Screening of an FDA-
576   approved compound library identifies four small-molecule inhibitors of Middle East
577   respiratory syndrome coronavirus replication in cell culture. Antimicrob Agents
578   Chemother 58:4875-84.
579 49. Agostini ML, Andres EL, Sims AC, Graham RL, Sheahan TP, Lu X, Smith EC, Case JB,
580   Feng JY, Jordan R, Ray AS, Cihlar T, Siegel D, Mackman RL, Clarke MO, Baric RS,
581   Denison MR. 2018. Coronavirus Susceptibility to the Antiviral Remdesivir (GS-5734) Is
582   Mediated by the Viral Polymerase and the Proofreading Exoribonuclease. MBio 9.
583 50. Jordheim LP, Durantel D, Zoulim F, Dumontet C. 2013. Advances in the development of
584   nucleoside and nucleotide analogues for cancer and viral diseases. Nat Rev Drug Discov
585   12:447-64.
586 51. de Wilde AH, Raj VS, Oudshoorn D, Bestebroer TM, van Nieuwkoop S, Limpens R,
587   Posthuma CC, van der Meer Y, Barcena M, Haagmans BL, Snijder EJ, van den Hoogen
588   BG. 2013. MERS-coronavirus replication induces severe in vitro cytopathology and is
589   strongly inhibited by cyclosporin A or interferon-alpha treatment. J Gen Virol 94:1749-
590   1760.
591 52. Knaap RCM, Fernández-Delgado R, Dalebout TJ, Oreshkova N, Bredenbeek PJ,
592   Enjuanes L, Sola I, Snijder EJ, Kikkert M. 2019. The deubiquitinating activity of Middle
593   East respiratory syndrome coronavirus papain-like protease delays the innate immune
594   response and enhances virulence in a mouse model. bioRxiv doi:10.1101/751578:751578.
595 53. El-Awady R, Saleh E, Hashim A, Soliman N, Dallah A, Elrasheed A, Elakraa G. 2016.
596   The Role of Eukaryotic and Prokaryotic ABC Transporter Family in Failure of
597   Chemotherapy. Front Pharmacol 7:535.
598 54. Menachery VD, Mitchell HD, Cockrell AS, Gralinski LE, Yount BL, Jr., Graham RL,
599   McAnarney ET, Douglas MG, Scobey T, Beall A, Dinnon K, 3rd, Kocher JF, Hale AE,
600   Stratton KG, Waters KM, Baric RS. 2017. MERS-CoV Accessory ORFs Play Key Role
601   for Infection and Pathogenesis. mBio 8.
602 55. Liu DX, Fung TS, Chong KK, Shukla A, Hilgenfeld R. 2014. Accessory proteins of
603   SARS-CoV and other coronaviruses. Antiviral Res 109:97-109.
604 56. Mou H, Raj VS, van Kuppeveld FJ, Rottier PJ, Haagmans BL, Bosch BJ. 2013. The
605   receptor binding domain of the new Middle East respiratory syndrome coronavirus maps
606   to a 231-residue region in the spike protein that efficiently elicits neutralizing antibodies.
607   J Virol 87:9379-83.
608 57. Hoffmann M, Mosbauer K, Hofmann-Winkler H, Kaul A, Kleine-Weber H, Kruger N,
609   Gassen NC, Muller MA, Drosten C, Pohlmann S. 2020. Chloroquine does not inhibit
610   infection of human lung cells with SARS-CoV-2. Nature 585:588-590.
611 58. Lau SK, Lau CC, Chan KH, Li CP, Chen H, Jin DY, Chan JF, Woo PC, Yuen KY. 2013.
612   Delayed induction of proinflammatory cytokines and suppression of innate antiviral
613   response by the novel Middle East respiratory syndrome coronavirus: implications for
614   pathogenesis and treatment. J Gen Virol 94:2679-90.
615 59. Kusaka T, Yamamoto H, Shibata M, Muroi M, Kishi T. 1968. Streptomyces citricolor
616   nov. sp. and a new antibiotic, aristeromycin. J Antibiot (Tokyo) 21:255-63.

617   60.   Wolfe MS, Lee Y, Bartlett WJ, Borcherding DR, Borchardt RT. 1992. 4'-modified
618   analogues of aristeromycin and neplanocin A: synthesis and inhibitory activity toward S-
619   adenosyl-L-homocysteine hydrolase. J Med Chem 35:1782-91.
620   61.   WANG JR, R. K.; CHU, C. K. 2011. Recent Advances in Carbocyclic Nucleosides:
621   Synthesis and Biological Activity. Med Chem Nucleic Acids
622   doi:10.1002/chin.201204251:1-100.
623   62.   Kloor D, Fuchs S, Petroktistis F, Delabar U, Muhlbauer B, Quast U, Osswald H. 1998.
624   Effects of ions on adenosine binding and enzyme activity of purified S-
625   adenosylhomocysteine hydrolase from bovine kidney. Biochem Pharmacol 56:1493-6.
626   63.   Hasobe M, McKee JG, Borchardt RT. 1989. Relationship between intracellular
627   concentration of S-adenosylhomocysteine and inhibition of vaccinia virus replication and
628   inhibition of murine L-929 cell growth. Antimicrob Agents Chemother 33:828-34.
629   64.   Ransohoff RM, Narayan P, Ayers DF, Rottman FM, Nilsen TW. 1987. Priming of
630   influenza mRNA transcription is inhibited in CHO cells treated with the methylation
631   inhibitor, neplanocin A. Antiviral Res 7:317-27.
632   65.   Kovacikova K, Morren BM, Tas A, Albulescu IC, van Rijswijk R, Jarhad DB, Shin YS,
633   Jang MH, Kim G, Lee HW, Jeong LS, Snijder EJ, van Hemert MJ. 2020. 6'-beta-Fluoro-
634   Homoaristeromycin and 6'-Fluoro-Homoneplanocin A Are Potent Inhibitors of
635   Chikungunya Virus Replication through Their Direct Effect on Viral Nonstructural
636   Protein 1. Antimicrob Agents Chemother 64.
637   66.   Chen H, Zhou B, Brecher M, Banavali N, Jones SA, Li Z, Zhang J, Nag D, Kramer LD,
638   Ghosh AK, Li H. 2013. S-adenosyl-homocysteine is a weakly bound inhibitor for a
639   flaviviral methyltransferase. PLoS One 8:e76900.
640   67.   Jin X, Chen Y, Sun Y, Zeng C, Wang Y, Tao J, Wu A, Yu X, Zhang Z, Tian J, Guo D.
641   2013. Characterization of the guanine-N7 methyltransferase activity of coronavirus nsp14
642   on nucleotide GTP. Virus Res 176:45-52.
643   68.   Aouadi W, Eydoux C, Coutard B, Martin B, Debart F, Vasseur JJ, Contreras JM, Morice
644   C, Querat G, Jung ML, Canard B, Guillemot JC, Decroly E. 2017. Toward the
645   identification of viral cap-methyltransferase inhibitors by fluorescence screening assay.
646   Antiviral Res 144:330-339.
647   69.   Chiang PK. 1998. Biological effects of inhibitors of S-adenosylhomocysteine hydrolase.
648   Pharmacol Ther 77:115-34.
649   70.   Decroly E, Debarnot C, Ferron F, Bouvet M, Coutard B, Imbert I, Gluais L,
650   Papageorgiou N, Sharff A, Bricogne G, Ortiz-Lombardia M, Lescar J, Canard B. 2011.
651   Crystal structure and functional analysis of the SARS-coronavirus RNA cap 2'-O-
652   methyltransferase nsp10/nsp16 complex. PLoS Pathog 7:e1002059.
653   71.   Shannon A, Fattorini V, Sama B, Selisko B, Feracci M, Falcou C, Gauffre P, Kazzi PE,
654   Decroly E, Rabah N, Alvarez K, Eydoux C, Guillemot J-C, Debart F, Vasseur J-J, Noel
655   M, Moussa A, Good S, Lin K, Sommadossi J-P, Zhu Y, Yan X, Shi H, Ferron F, Canard
656   B. 2021. Protein-primed RNA synthesis in SARS-CoVs and structural basis for inhibition
657   by AT-527. bioRxiv doi:10.1101/2021.03.23.436564:2021.03.23.436564.
658   72.   Slanina H, Madhugiri R, Bylapudi G, Schultheiss K, Karl N, Gulyaeva A, Gorbalenya
659   AE, Linne U, Ziebuhr J. 2021. Coronavirus replication-transcription complex: Vital and
660   selective NMPylation of a conserved site in nsp9 by the NiRAN-RdRp subunit. Proc Natl
661   Acad Sci U S A 118.
662   73.   Yan L, Ge J, Zheng L, Zhang Y, Gao Y, Wang T, Huang Y, Yang Y, Gao S, Li M, Liu Z,
663   Wang H, Li Y, Chen Y, Guddat LW, Wang Q, Rao Z, Lou Z. 2021. Cryo-EM Structure

664   of an Extended SARS-CoV-2 Replication and Transcription Complex Reveals an
665   Intermediate State in Cap Synthesis. Cell 184:184-193 e10.
666 74. Hao W, Wojdyla JA, Zhao R, Han R, Das R, Zlatev I, Manoharan M, Wang M, Cui S.
667   2017. Crystal structure of Middle East respiratory syndrome coronavirus helicase. PLoS
668   Pathog 13:e1006474.
669 75. Yan L, Zhang Y, Ge J, Zheng L, Gao Y, Wang T, Jia Z, Wang H, Huang Y, Li M, Wang
670   Q, Rao Z, Lou Z. 2020. Architecture of a SARS-CoV-2 mini replication and transcription
671   complex. Nat Commun 11:5874.
672 76. Urakova N, Kuznetsova V, Crossman DK, Sokratian A, Guthrie DB, Kolykhalov AA,
673   Lockwood MA, Natchus MG, Crowley MR, Painter GR, Frolova EI, Frolov I. 2018.
674   beta-d-N (4)-Hydroxycytidine Is a Potent Anti-alphavirus Compound That Induces a
675   High Level of Mutations in the Viral Genome. J Virol 92.
676 77. Agostini ML, Pruijssers AJ, Chappell JD, Gribble J, Lu X, Andres EL, Bluemling GR,
677   Lockwood MA, Sheahan TP, Sims AC, Natchus MG, Saindane M, Kolykhalov AA,
678   Painter GR, Baric RS, Denison MR. 2019. Small-Molecule Antiviral beta-d-N (4)-
679   Hydroxycytidine Inhibits a Proofreading-Intact Coronavirus with a High Genetic Barrier
680   to Resistance. J Virol 93.
681 78. Shannon A, Selisko B, Le NT, Huchting J, Touret F, Piorkowski G, Fattorini V, Ferron F,
682   Decroly E, Meier C, Coutard B, Peersen O, Canard B. 2020. Rapid incorporation of
683   Favipiravir by the fast and permissive viral RNA polymerase complex results in SARS-
684   CoV-2 lethal mutagenesis. Nat Commun 11:4682.
685 79. Meier C, Balzarini J. 2006. Application of the cycloSal-prodrug approach for improving
686   the biological potential of phosphorylated biomolecules. Antiviral Res 71:282-92.
687 80. Shin YS, Jarhad DB, Jang MH, Kovacikova K, Kim G, Yoon JS, Kim HR, Hyun YE,
688   Tipnis AS, Chang TS, van Hemert MJ, Jeong LS. 2020. Identification of 6'-beta-fluoro-
689   homoaristeromycin as a potent inhibitor of chikungunya virus replication. Eur J Med
690   Chem 187:111956.
691 81. De Clercq E. 1998. Carbocyclic adenosine analogues as S-adenosylhomocysteine
692   hydrolase inhibitors and antiviral agents: recent advances. Nucleosides Nucleotides
693   17:625-34.
694 82. Bray M, Driscoll J, Huggins JW. 2000. Treatment of lethal Ebola virus infection in mice
695   with a single dose of an S-adenosyl-L-homocysteine hydrolase inhibitor. Antiviral Res
696   45:135-47.
697 83. Huggins J, Zhang ZX, Bray M. 1999. Antiviral drug therapy of filovirus infections: S-
698   adenosylhomocysteine hydrolase inhibitors inhibit Ebola virus in vitro and in a lethal
699   mouse model. J Infect Dis 179 Suppl 1:S240-7.
700 84. De Fazio G, Alba AP, Vicente M, De Clercq E. 1990. Antiviral activity of S-
701   adenosylhomocysteine hydrolase inhibitors against plant viruses. Antiviral Res 13:219-
702   26.
703 85. De Clercq E, Cools M, Balzarini J, Marquez VE, Borcherding DR, Borchardt RT, Drach
704   JC, Kitaoka S, Konno T. 1989. Broad-spectrum antiviral activities of neplanocin A, 3-
705   deazaneplanocin A, and their 5'-nor derivatives. Antimicrob Agents Chemother 33:1291-
706   7.
707 86. Ogando NS, Zevenhoven-Dobbe JC, van der Meer Y, Bredenbeek PJ, Posthuma CC,
708   Snijder EJ. 2020. The enzymatic activity of the nsp14 exoribonuclease is critical for
709   replication of MERS-CoV and SARS-CoV-2. J Virol doi:10.1128/JVI.01246-20.

710   87.   Nedialkova DD, Gorbalenya AE, Snijder EJ. 2010. Arterivirus Nsp1 modulates the
711   accumulation of minus-strand templates to control the relative abundance of viral
712   mRNAs. PLoS Pathog 6:e1000772.
713   88.   Pfefferle S, Krahling V, Ditt V, Grywna K, Muhlberger E, Drosten C. 2009. Reverse
714   genetic characterization of the natural genomic deletion in SARS-Coronavirus strain
715   Frankfurt-1 open reading frame 7b reveals an attenuating function of the 7b protein in-
716   vitro and in-vivo. Virol J 6:131.
717   89.   Salgado-Benvindo C, Thaler M, Tas A, Ogando NS, Bredenbeek PJ, Ninaber DK, Wang
718   Y, Hiemstra PS, Snijder EJ, van Hemert MJ. 2020. Suramin Inhibits SARS-CoV-2
719   Infection in Cell Culture by Interfering with Early Steps of the Replication Cycle.
720   Antimicrob Agents Chemother 64.
721   90.   Lavi E, Gilden DH, Highkin MK, Weiss SR. 1984. Persistence of mouse hepatitis virus
722   A59 RNA in a slow virus demyelinating infection in mice as detected by in situ
723   hybridization. J Virol 51:563-6.
724   91.   Bryans JT, Crowe ME, Doll ER, McCollum WH. 1957. Isolation of a filterable agent
725   causing arteritis of horses and abortion by mares; its differentiation from the equine
726   abortion (influenza) virus. Cornell Vet 47:3-41.
727   92.   van den Worm SH, Eriksson KK, Zevenhoven JC, Weber F, Zust R, Kuri T, Dijkman R,
728   Chang G, Siddell SG, Snijder EJ, Thiel V, Davidson AD. 2012. Reverse genetics of
729   SARS-related coronavirus using vaccinia virus-based recombination. PLoS One
730   7:e32857.
731   93.   Ogando NS, Dalebout TJ, Zevenhoven-Dobbe JC, Limpens R, van der Meer Y, Caly L,
732   Druce J, de Vries JJC, Kikkert M, Barcena M, Sidorov I, Snijder EJ. 2020. SARS-
733   coronavirus-2 replication in Vero E6 cells: replication kinetics, rapid adaptation and
734   cytopathology. J Gen Virol doi:10.1099/jgv.0.001453.

735